Four-wheel Driving-force Distribution Method Based on Driving Stiffness and Slip Ratio Estimation for Electric Vehicle with In-wheel Motors

Kenta Maeda, Horishi Fujimoto and Yoichi Hori
The University of Tokyo
5–1–5 Kashiwanoha, Kashiwa, Chiba, Japan
Email: maeda@hflab.k.u-tokyo.ac.jp, fujimoto@k.u-tokyo.ac.jp, hori@k.u-tokyo.ac.jp

***Abstract*—In this paper, a four-wheel driving force distribution method based on driving stiffness and slip ratio estimation is proposed. In previously proposed distribution method, vehicle velocity is meaured by an expensive optical sensor and moreover the response speed of distribution is limited by that of Driving Force Control (DFC), the traction control proposed by the authors' research group. Therefore, driving stiffness and slip ratio estimation is applied to improve the distibution method. Due to the slip ratio estimation, vehicle velocity sensor is not needed and the distribution speed depends on that of driving stiffness estimation, which is faster than DFC. If the length of a slippery surface is shorter than the vehicle's wheel base, the total driving force is retained by distributing the shortage of driving force to the wheels that still have traction. On the other hand, when either the left or right side run on a slippery surface, yaw-moment is suppressed. The effectiveness of the improved method is verified by experiments.**

I. Introduction

As a solution for energy and environmental problems, electric vehicles (EVs) are receiving great attention. In addition, EVs have many advantages over internal combustion engine vehicles, since electric motors and inverters are utilized in EV drive systems. Their advantages can be summarized as follows [1]:

1) The torque response of electric motors is 100–500 times faster than that of engines.
2) All wheels can be controlled independently by adopting small high-power in-wheel motors.
3) The output torque of an electric motor can be measured accurately from the motor current.

Based on these advantages, many traction control methods for anti-skid on slippery surface have been proposed. Most of these methods are based on observers [2], [3], maximum transmissible torque estimation [4], slip ratio control [5], [6], sliding mode control [7]. In addition, since the maximum driving force that a wheel can generate on a surface is decided by the road friction μ, some methods have also been proposed to estimate μ [8], [9].

The authors' research group also has proposed traction control methods [10]–[12], and a four-wheel driving force distribution method based on Driving Force Control (DFC) is proposed [13]. However, the distribution method proposed in [13], is based on the control input of DFC and thus the response speed of distribution is limited by that of DFC. Moreover, an expensive optical sensor is also necessary for measuring high accuracy vehicle velocity.

Fig. 1. FPEV2-Kanon.

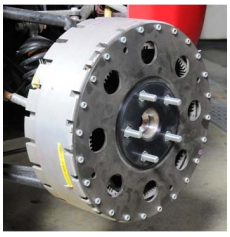

Fig. 2. In-wheel motor.

In this paper, driving stiffness of each wheel is estimated in order to improve the performance of driving-force distribution. In addition, in order to reduce the implemental cost, slip ratio estimation method is applied to estimate the vehicle velocity. The authors' research group has previously proposed slip ratio estimation methods on acceleration [10] and deceleration [11]. Since these two method differs because of the difference of slip ratio definition of between acceleration and deceleration, it is inconvenient for seamless control. In this paper, therefore, slip ratio estimation of deceleration [11] is applied to both acceleration and deceleration.

Applying the distribution method, total driving force is retained by distributing the shortage of driving force to wheels that still have traction even when a vehicle runs into a slippery road such as scattered snow or wet manholes, whose length is shorter than the vehicle's wheel base. Moreover, when either left or right side are on a slippery surface, yawing is suppressed by generating the difference between left and right driving force to follow desired yaw-moment — zero when running straight. The effectiveness of the proposed method is verified by experiments.

TABLE I
VEHICLE SPECIFICATIONS.

Vehicle Mass (m)	871 [kg]
Wheel Base (l)	1.7 [m]
Distance from C.G to Front Axle (l_f)	0.999 [m]
Distance from C.G to Rear Axle (l_r)	0.701 [m]
Tread Base (d_f, d_r)	1.3 [m]
Wheel Radius (r)	0.302 [m]

II. EXPERIMENTAL VEHICLE AND VEHICLE MODEL

A. Experimental Vehicle

The experimental EV "FPEV2-Kanon," developed by the authors' laboratory, is used for performance verification as shown in Fig. 1. In this section the characteristics of the experimental vehicle are explained.

Outer-rotor-type in-wheel motors as shown in Fig. 2 are installed in each wheel. Since these motors adopt direct drive system, reaction forces from the road are directly transferred to the motors without gear reduction or backlash. The maximum torque of each of the front motors is ± 500 [Nm], and that of the rear is ± 340 [Nm]. Additionally, an optical sensor is installed to measure the vehicle velocity accurately. The vehicle's specification is shown in Table I.

B. Equations of Vehicle Dynamics

In this section, equations of vehicle dynamics are explained [13].

The equation of rotational motion of each wheel is shown in Fig. 3 and can be described as

$$J_{ij}\dot{\omega}_{ij} = T_{ij} - rF_{dij}, \tag{1}$$

where J is the wheel inertia, ω is the wheel angular velocity, T is the motor torque, r is the wheel radius, F_d is the driving force at the point where the wheel makes contact with the ground. Also, i and j are indices for f/r (front/rear) and l/r (left/right) respectively. The equation of longitudinal motion of the vehicle body is shown in Fig. 4 and can be described as

$$\begin{aligned} m\dot{V} &= F_{dfl} + F_{dfr} + F_{drl} + F_{drr} \\ &= F_{dall}, \end{aligned} \tag{2}$$

where m is the vehicle mass, V is the vehicle velocity, F_{dall} is the total driving force. When the vehicle accelerates or decelerates, the wheel velocity $V_\omega = r\omega$ differs from the vehicle velocity V. The slip ratio λ is defined as

$$\lambda = \frac{V_\omega - V}{\max(V_\omega, V, \epsilon)}, \tag{3}$$

where ϵ is a tiny value to prevent division by zero. The driving force F_d and the driving stiffness D_s at each wheel are obtained as

$$F_{dij} = \mu_{ij} N_{ij}, \tag{4}$$

$$D_{sij} = \left.\frac{dF_{dij}}{d\lambda_{ij}}\right|_{\lambda_{ij}=0}, \tag{5}$$

where N is the normal reaction force on each wheel, and μ is the friction coefficient.

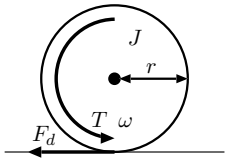

Fig. 3. Rotational motion of wheel.

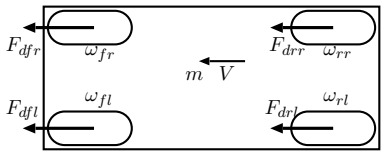

Fig. 4. Variables in vehicle motion.

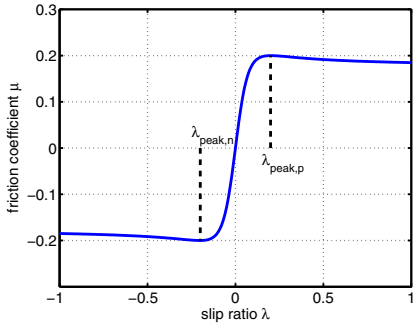

Fig. 5. Typical μ-λ relationship.

The relationship between μ and λ depends on the road condition, and is known to be as Fig. 5 [14]. There are $\lambda_{\mathrm{peak,p}}$, $\lambda_{\mathrm{peak,n}}$ on which μ is the maximum or the minimum. In the domain of $\lambda_{\mathrm{peak,n}} \leq \lambda \leq \lambda_{\mathrm{peak,p}}$, μ is a monotonically increasing function of λ, and outside the domain, a monotonically decreasing function.

III. DRIVING FORCE CONTROL

In this section, the driving force control (DFC) method is explained [13]. The block diagram of DFC is shown in Fig. 6. The outer loop is a driving force loop based on driving force observer and the inner loop is a wheel velocity loop that controls the slip ratio. F_d^* is the driving force reference and $\hat{F}_d$ is the driving force estimated with motor torque reference T^* and wheel velocity ω, assuming that current control of motor is fast enough for $T = T^*$ to be valid.

Since the definition of slip ratio λ for acceleration ($V_\omega \geq V$) differs from that of the definition for deceleration ($V_\omega < V$), λ is inconvenient to control. Therefore, instead of the slip ratio, the control input y, defined as follows, is controlled.

$$y = \frac{V_\omega}{V} - 1. \tag{6}$$

This is the same definition as the definition of slip ratio for deceleration. The relationship between λ and y in the domain of $\lambda > 0$ is calculated as

$$y = \frac{\lambda}{1-\lambda}, \tag{7}$$

which indicates that y equals to λ when $|\lambda| \ll 1$ and they are always one to one correspondence.

From (6), the wheel velocity reference V_ω^* of the inner loop is calculated as

$$V_\omega^* = (1+y)V, \tag{8}$$

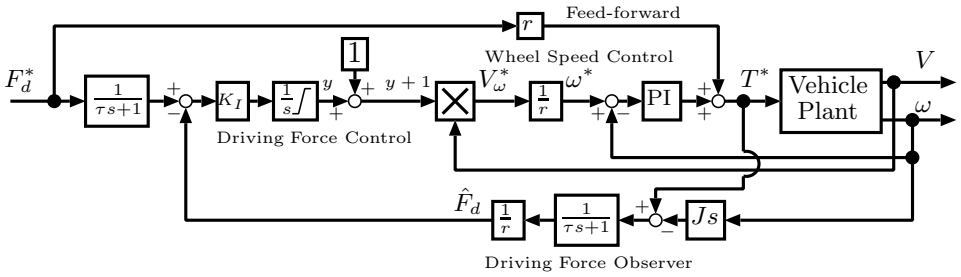

Fig. 6. Block diagram of DFC.

which shows that the vehicle cannot start moving from a standstill ($V = 0$) since V_ω^* is equal to 0 reagrdless of y. To prevent this problem, the reference V_ω^* is modified where V is smaller than a given constant σ as follows:

$$\begin{cases} V_\omega^* = V + y\sigma & (V < \sigma), \\ V_\omega^* = V + yV & (V \geq \sigma). \end{cases} \tag{9}$$

The driving force controller, whose initial value is set as $y_0 = 0$, is designed as integration (I) control with gain K_I. Saturation is applied to the integrator output for limiting y to $y_{\min} \leq y \leq y_{\max}$. With this saturation, traction can be retained by keeping the slip ratio within the domain where μ is a monotonic function of λ.

IV. Proposed Method

A. Slip Ratio Estimator

The authors' research group has proposed the slip ratio estimation method without sensing vehicle velocity. Two different methods have been proposed because the definition of slip ratio on acceleration differs from that on deceleration, which is inconvenient for seamless control of acceleration and deceleration. In this paper, therefore, the estimation method on deceleration is applied to the driving force control both on acceleration and deceleration.

By differentiating (3) and substituting (2) into it, the state equation of λ is obtained as

$$\dot{\lambda}_{ij} = \frac{\dot{\omega_{ij}}}{\omega_{ij}}(1 + \lambda_{ij}) - \frac{F_{dall}}{r^2 \omega_{ij} M}(1 + \lambda_{ij})^2. \tag{10}$$

Although F_{dall} in (10) contains running resistance, driving force observer cannot estimate it. Therefore, instead of using $\hat{F}_{dall}$, vehicle longitudinal acceleration a_x is employed for slip ratio estimator (SRE) as follows:

$$\dot{\hat{\lambda}}_{ij} = \frac{\dot{\omega}_{ij}}{\omega_{ij}}(1 + \hat{\lambda}_{ij}) - \frac{a_x}{r^2 \omega_{ij}}(1 + \hat{\lambda}_{ij})^2. \tag{11}$$

Vehicle velocity on each wheel for DFC is calculated by the estimated slip ratio $\hat{\lambda}_{ij}$ as

$$V_{ij} = \frac{r\omega_{ij}}{1 + \hat{\lambda}_{ij}}. \tag{12}$$

B. Driving Force Distribution Method

In this section, four-wheel driving force distribution is explained. When slip ratio λ increases on a slippery surface and the control input y of DFC approaches to the upper limit, driving force is saturated and reduced. To avoid this reduction, λ of each wheel needs to be small enough to prevent saturation. Therefore, the proposed method decides the driving force reference of each wheel to minimize λ of each wheel, satisfying total driving force reference F_{dall}^* and yaw-moment reference M_z^* generated by driving force difference.

The relationship between driving force of each wheel F_{dij} and F_{dall}, M_z is as follows:

$$\begin{bmatrix} 1 & 1 & 1 & 1 \\ -\frac{d_f}{2} & \frac{d_f}{2} & -\frac{d_r}{2} & \frac{d_r}{2} \end{bmatrix} \begin{bmatrix} F_{dfl} \\ F_{dfr} \\ F_{drl} \\ F_{drr} \end{bmatrix} = \begin{bmatrix} F_{dall} \\ M_z \end{bmatrix}. \tag{13}$$

Here, by setting the coefficient matrix in the left-hand side as $\boldsymbol{A}$, the vector of driving force of each wheel $[F_{dfl}, F_{dfr}, F_{drl}, F_{drr}]^T$ as $\boldsymbol{x}$, and that of total driving force and yaw-moment $[F_{dall}, M_z]^T$ as $\boldsymbol{b}$, (13) can be rewritten as $\boldsymbol{Ax} = \boldsymbol{b}$. From (5) driving stiffness of each wheel D_{sij} in the domain of $|\lambda| \ll 1$ can be obtained as

$$D_{sij} = \frac{F_{dij}}{\lambda_{ij}}. \tag{14}$$

Then the cost function J is defined as the sum of squares of slip ratio λ_{ij}.

$$\begin{aligned} J &= \lambda_{fl}^2 + \lambda_{fr}^2 + \lambda_{rl}^2 + \lambda_{rr}^2 \\ &= \frac{F_{dfl}^2}{D_{sfl}^2} + \frac{F_{dfr}^2}{D_{sfr}^2} + \frac{F_{drl}^2}{D_{srl}^2} + \frac{F_{drr}^2}{D_{srr}^2}. \end{aligned} \tag{15}$$

Therefore, the weighted least squares solution $\boldsymbol{x_{opt}}$ of (13) that minimizes J, and weighting matrix $\boldsymbol{W}$ are as follows.

$$\boldsymbol{x_{opt}} = \boldsymbol{W}^{-1}\boldsymbol{A}^T(\boldsymbol{A}\boldsymbol{W}^{-1}\boldsymbol{A}^T)^{-1}\boldsymbol{b}, \tag{16}$$

$$\boldsymbol{W} = \mathrm{diag}\left(\frac{1}{D_{sfl}^2}, \frac{1}{D_{sfr}^2}, \frac{\phi_r}{D_{srl}^2}, \frac{\phi_r}{D_{srr}^2}\right). \tag{17}$$

Here, ϕ_r is the tuning gain which adjust front and rear driving force distribution ratio. Larger amount of driving force is distributed to rear wheels than front ones during acceleration, which possibly leads to excessive driving force references on

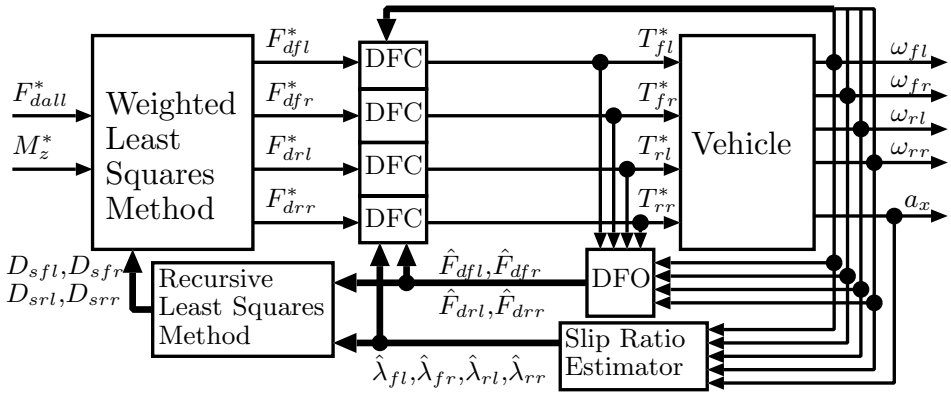

Fig. 7. The block diagram of proposed method.

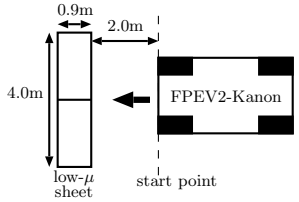

Fig. 8. Instantaneous low-μ road.

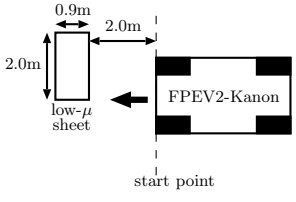

Fig. 9. Split low-μ road.

rear wheels over the upper limit of rear motor torque and total driving force saturates even on a high-μ surface. Therefore ϕ_r is set as $\phi_r \geq 1$ during acceleration to prevent the saturation.

C. Driving Stiffness Estimation

From (14), the relationship between F_d and λ is $F_d = D_s\lambda$. Therefore, the driving stiffness of each wheel at sample k $D_{sij}(k)$ can be estimated by the Recursive Least Squares (RLS) algorithm as follows [12]:

$$\hat{D}_{sij}(k) = \hat{D}_{sij}(k-1) - \frac{\Gamma(k-1)\lambda(k)}{w+\lambda_{ij}(k)\Gamma(k-1)\lambda_{ij}(k)} \times \left[\lambda_{ij}(k)\hat{D}_{sij}(k-1) - \hat{F}_{dij}(k)\right] \quad (18)$$

$$\Gamma(k) = \frac{1}{w}\left[\Gamma(k-1) - \frac{\Gamma(k-1)\lambda_{ij}(k)^2\Gamma(k-1)}{w+\lambda_{ij}(k)\Gamma(k-1)\lambda_{ij}(k)}\right] \quad (19)$$

where w is the forgetting factor. If regressor $\lambda_{ij}(k)$ equals zero, the persistent excitation is not satisfied. Therefore $\hat{D}_{sij}(k)$ and $\Gamma(k)$ are not updated if $|\lambda_{ij}(k)| < 0.005$. Lower limitations 1000 are imposed to $\hat{D}_{sij}$ avoiding division by zero in (17).

Fig. 7 shows the block diagram of the whole system. The driving force references F^*_{dij} are given by $\boldsymbol{x_{opt}}$.

V. Experiments

A. Experimental Setup

In this section, experimental results are explained. A polymer sheet is utilized to simulate slippery road condition. This sheet, called "low-μ sheet" in this paper, can realize a friction coefficient μ of about 0.2 by watering on it.

As shown in Fig. 8 and Fig. 9, the low-μ sheet of length 0.9 [m], shorter than the wheel base of "FPEV2-Kanon", is set at the distance of 2.0 [m] from the start point. The experimental vehicle starts at the start point and accelerates with total driving force reference $F^*_{dall} = 2000$ [Nm]. The parameters are, $K_I = 0.01$, $\tau = 30$ [ms], $y_{\min} = 0.2$ and $y_{\max} = 0.25$ which corresponds to a slip ratio of $\lambda = \pm 0.2$. The wheel speed PI controller is designed by the pole assignment method towards the plant $\frac{1}{Js}$, which is from (1) ignoring F_d, setting the pole -20 [rad/s]. All parameters are the same for each wheel.

The parameters of driving force distribution method are, forgetting factor is $w = 0.995$, tuning gain is $\phi_r = 1.3$, and the integrator output of SRE is limited from -0.3 to 0.43, which corresponds to a slip ratio of $\lambda = \pm 0.3$.

B. Slip Ratio Estimation

In this section, the slip ratio estimation method is verified by experimental results. Fig. 10 is the results of acceleration test on instantaneous slippery surface as shown in Fig. 8. Vehicle velocity is measured using an optical sensor to calculate true slip ratio of each wheel. Since SRE estimates the slip ratio during deceleration, estimated slip ratio shown in Fig. 10(b) is the converted value by the same relational expression as (7).

Fig. 10(a) shows the true slip ratio calculated by measured vehicle velocity and wheel speed. The result before 1.2 [s] is not correct because the optical sensor used in this paper cannot measure velocity accurately on low speed. The estimated slip ratio shown in Fig. 10(b) is also not accurate during that period. It is considered to be because the slip ratio calculation is close to the division of zero by zero on low speed. Notwithstanding, the estimated slip ratio gradually converges and corresponds to the true value after 2.0[s] as shown in Fig. 10(c), which is the comparison of the measured and estimated slip ratio on the front right wheel. From Fig. 10(d), it can be confirmed that the estimated vehicle velocity matches with the measures value very well.

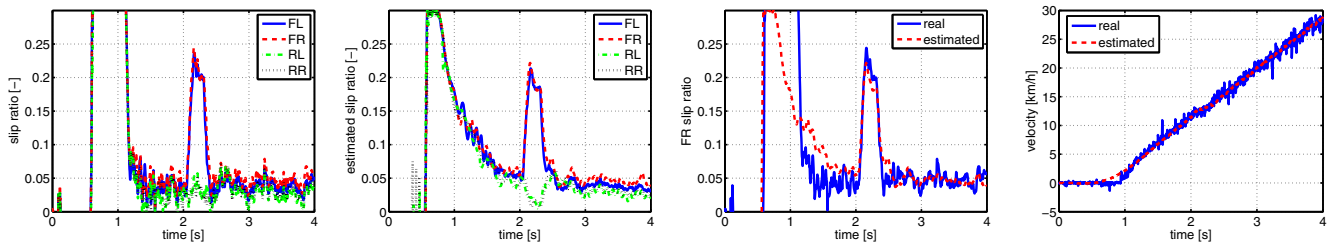

(a) λ on each wheel. (b) Estimated $\hat{\lambda}$ on each wheel. (c) Comparing λ_{fr} with $\hat{\lambda}_{fr}$. (d) Vehicle velocity.

Fig. 10. Results of slip ratio estimation.

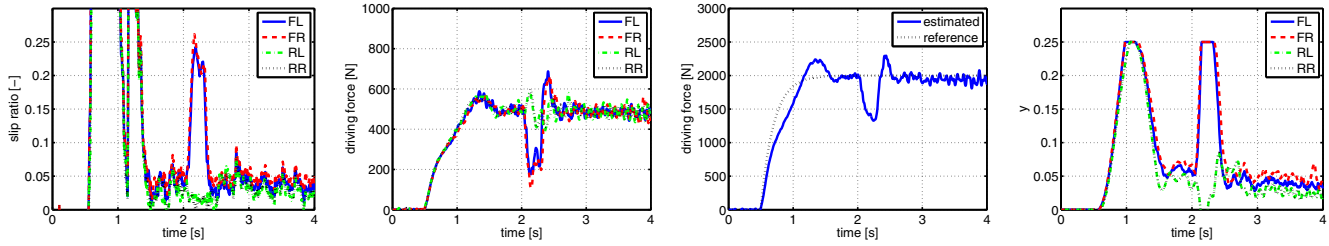

(a) λ on each wheel. (b) $\hat{F}_d$ on each wheel. (c) $\hat{F}_{dall}$. (d) y on each wheel.

Fig. 11. Experiment of instantaneous slippery road (only DFC)

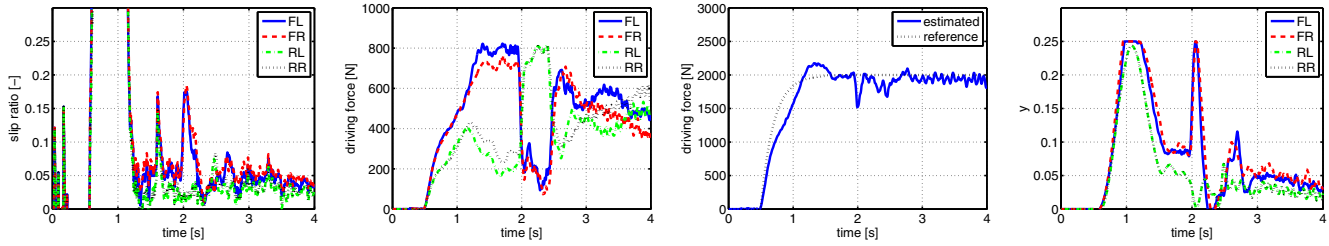

(a) λ on each wheel. (b) $\hat{F}_d$ on each wheel. (c) $\hat{F}_{dall}$. (d) y on each wheel.

Fig. 12. Experiment of instantaneous slippery road (proposed)

C. Instantaneous Slippery Road

The experimental results on the instantaneous slippery surface are shown in Fig. 11 and Fig. 12. In each result, front wheels are on slippery surface from about 2.0 [s] to 2.3 [s], and rear ones are on slippery surface from about 2.5 [s] to 2.7 [s].

Fig. 11 shows the results of the conventional method with DFC and SRE on each wheel and without driving force distribution, i.e., driving force references on each wheel are the same. Fig. 11(a) shows that the front slip ratio increases to about 0.2 when passing over the slippery surface, As a result, the front driving force decreases as shown in Fig. 11(b), which leads to the diminution of the total driving force as shown in Fig. 11(c).

Fig. 12 shows the results of the proposed method with DFC, SRE and the driving-force distribution. Compared to the conventional method, Fig. 12(a) shows that the front slip ratio is suppressed to no more than 0.15 and immediately decreases even on the slippery surface. Front and rear driving forces are compensated for each other as shown in Fig. 12(b), and consequently the total driving force is retained to the reference as shown in Fig. 12(c). As for the control input y of DFC, front y saturates to the upper limit 0.25 when the front wheels are on slippery surface as shown in Fig. 11(d). Compared to it, proposed method prevents this saturation as shown in Fig. 12(d).

Rear wheels do not reduce their driving force by the conventional method as shown in Fig. 11(b). This is because the rear static load of "FPEV2-Kanon" is larger than the front one. Moreover, load is transfered to rear axis during acceleration.

D. Split Slippery Road

The experimental results on the split slippery surface are shown in Fig. 13 and Fig. 14. In each result, front-right wheel is on slippery surface from about 2.0 [s] to 2.3 [s], and rear-right one is on slippery surface from about 2.5 [s] to 2.7 [s].

Similar to section V-C, Fig. 13 shows the results of the conventional method and Fig. 14 shows those of the proposed one. Fig. 13(a) shows that only the front-right slip ratio increases to about 0.2 when passing over the slippery surface. As a result, only the front-right driving force decreases as shown in Fig. 13(b), which leads to the diminution of the total driving force as shown in Fig. 13(c) and the generation of the undesired yaw-moment of about -200 [Nm] as shown in Fig. 13(d).

Compared to the conventional method, Fig. 14(a) shows that

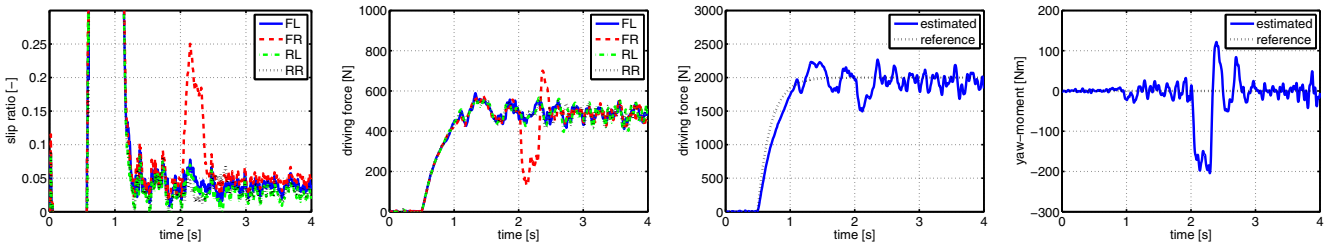

(a) λ on each wheel. (b) $\hat{F}_d$ on each wheel. (c) $\hat{F}_{dall}$. (d) $\hat{M}_z$.

Fig. 13. Experiment of instantaneous slippery road (only DFC)

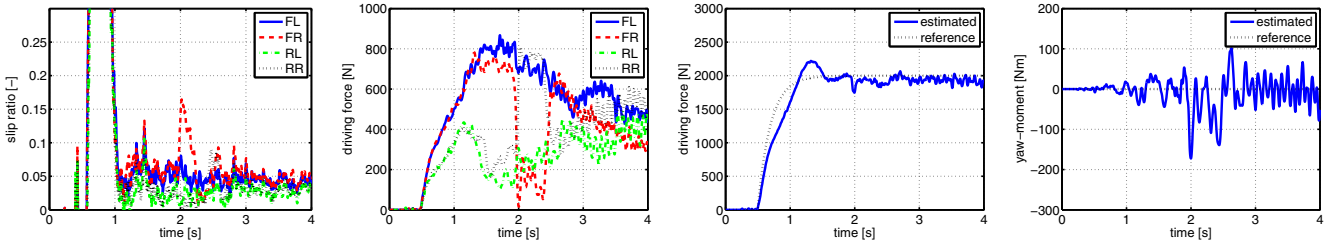

(a) λ on each wheel. (b) $\hat{F}_d$ on each wheel. (c) $\hat{F}_{dall}$. (d) $\hat{M}_z$.

Fig. 14. Experiment of instantaneous slippery road (proposed)

the front-right slip ratio is suppressed to no more than 0.15 and immediately decreases despite on the slippery surface. The front-right and the rear-right driving force is compensated for each other as shown in Fig. 14(b), and consequently the total driving force is retained to the reference as shown in Fig. 14(c). Also the undesired yaw-moment is suppressed as shown in Fig. 14(d).

VI. Conclusion

In this paper, four-wheel driving force distribution method based on driving stiffness and slip ratio estimation is proposed, and its effectiveness is verified by experiments. With the proposed distribution method, the reduction of total driving force and generation of yaw-moment is prevented very quickly without sensing the vehicle velocity by an expensive optical sensor. Due to the proposed method, EVs can be driven without difficulty no matter what road condition.

In future, the authors' research group plans to consider deceleration and cornering, and to estimate λ_{peak} in realtime based on DFC.

Acknowledgment

This research was partly supported by the Industrial Technology Research Grant Program from the New Energy and Industrial Technology Development Organization (NEDO) of Japan (number 05A48701d), and by the Ministry of Education, Culture, Sports, Science and Technology grant (number 22246057).

References

[1] Y. Hori, "Future vehicle driven by electricity and control—research on four-wheel-motored "UOT Electric March II"", *IEEE Trans. Industrial Electronics*, Vol. 51, No. 5, pp. 954–962, 2004.

[2] D. Foito, M. Guerreiro, A. Cordeiro, "Anti-slip wheel controller drive for EV using speed and torque observers", in *Proc. the 18th International Conference on Electrical Machines*, pp. 1–5, 2008.

[3] Y. Ge, C. S. Chang, "Torque distribution control for electric vehicle based on traction force observer", in *Proc. the IEEE International Conference on Computer Science and Automation Engineering*, pp. 371–375, 2011.

[4] J. Hu, D. Yin, Y. Hori, and F. Hu, "Electric vehicle traction control: A new mtte methodology," *IEEE Industry Applications Magazine*, vol. 18, no. 2, pp. 23–31, 2012.

[5] M. Kamachi, H. Miyamoto, and H. Yoshida, "Development of electric vehicle for on-road test," in *Proceedings of 9th International Symposium on Advanced Vehicle Control*, pp. 665–669, 2008.

[6] G. Zou, Y. Luo, K. Li, and X. Lian, "Slip ratio control of independent awd ev based on fuzzy dsmc," in *Proceedings of ICVES. IEEE International Conference on Vehicular Electronics and Safety 2007*, pp. 1–6, 2007.

[7] K. Xu, G. Xu, W. Li, L. Jian, and Z. Song, "Anti-skid for electric vehicles based on sliding mode control with novel structure," in *Proceedings of 2011 IEEE International Conference on Information and Automation*, pp. 650–655, 2011.

[8] R. Hoseinnezhad and A. Bab-Hadiashar, "Efficient antilock braking by direct maximization of tire-road frictions," *IEEE Transactions on Industrial Electrinics*, vol. 58, no. 8, pp. 3593–3600, 2011.

[9] G. Erdogan, L. Alexander, and R. Rajamani, "Estimation of tire-road friction coefficient using a novel wireless piezoelectric tire sensor," *IEEE Sensors Journal*, vol. 11, no. 2, pp. 267–279, 2011.

[10] K. Fujii, H. Fujimoto and N. Takahashi, "Vehicle stability control of electric vehicle with slip-ratio and cornering stiffness estimation", in *Proceedings of IEEE/ASME International Conference on Advanced Intelligent Mechatronics*, pp. 27–32, 2007.

[11] T. Suzuki and H. Fujimoto, "Slip ratio estimation and regenerative brake control without detection of vehicle velocity and acceleration for electric vehicle at urgent brake-turning", in *Proceedings of the 11th IEEE International Workshop on Advanced Motion Control*, pp. 273–278, 2010.

[12] T. Kanou and H. Fujimoto, "Slip-ratio based yaw-rate control with driving stiffness identification for electric vehicle," in *Proceedings of 9th International Symposium on Advanced Vehicle Control*, pp. 786–791, 2008.

[13] K. Maeda, H. Fujimoto and Y. Hori, "Four-wheel Driving-force Distribution Method for Instantaneous or Split Slippery Roads for Electric Vehicle with In-wheel Motors", in *Proceedings of The 12th International Workshop on Advanced Motion Control*, pp. 1–6, 2012.

[14] H. B. Pacejka and E. Bakker, "The magic formula tyre model", Tyre models for vehicle dynamic analysis: in *Proc. the 1st International Colloquium on Tyre Models for Vehicle Dynamics Analysis, held in Delft, The Netherlands*, pp. 1–18, 1991.